ACS APPLIED MATERIALS & INTERFACES
Research Article
www.acsami.org

Impact of Interlayer Processing Conditions on the Performance of GaN Light-Emitting Diode with Specific NiO_x/Graphene Electrode

S. Chandramohan,[†] Ji Hye Kang,[†] Beo Deul Ryu,[†] Jong Han Yang,[†] Seongjun Kim,[†] Hynsoo Kim,[†] Jong Bae Park,[‡] Taek Yong Kim,[§] Byung Jin Cho,[§] Eun-Kyung Suh,[†] and Chang-Hee Hong*,[†]

[†]School of Semiconductor and Chemical Engineering, Semiconductor Physics Research Center, Chonbuk National University, Jeonju 561-756, South Korea

[‡]Korea Basic Science Institute (KBSI), Jeonju Center, 664-14 Dukjin dong 1-ga, Dukjin-gu, Jeonju 561-756, South Korea

[§]Department of Electrical Engineering, KAIST, 291 Daehak-ro, Yuseong-gu, Daejeon 305 701, South Korea

Supporting Information

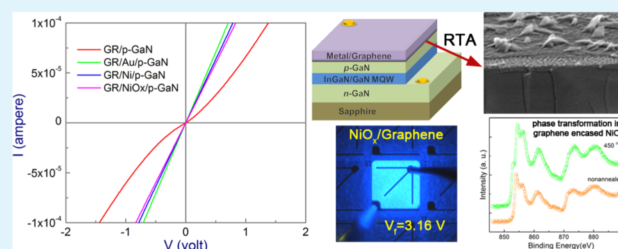

ABSTRACT: This paper reports on the evaluation of the impact of introducing interlayers and postmetallization annealing on the graphene/p-GaN ohmic contact formation and performance of associated devices. Current−voltage characteristics of the graphene/p-GaN contacts with ultrathin Au, Ni, and NiO_x interlayers were studied using transmission line model with circular contact geometry. Direct graphene/p-GaN interface was identified to be highly rectifying and postmetallization annealing improved the contact characteristics as a result of improved adhesion between the graphene and the p-GaN. Ohmic contact formation was realized when interlayer is introduced between the graphene and p-GaN followed by postmetallization annealing. Temperature-dependent $I-V$ measurements revealed that the current transport was modified from thermionic field emission for the direct graphene/p-GaN contact to tunneling for the graphene/metal/p-GaN contacts. The tunneling mechanism results from the interfacial reactions that occur between the metal and p-GaN during the postmetallization annealing. InGaN/GaN light-emitting diodes with NiO_x/graphene current spreading electrode offered a forward voltage of 3.16 V comparable to that of its Ni/Au counterpart, but ended up with relatively low light output power. X-ray photoelectron spectroscopy provided evidence for the occurrence of phase transformation in the graphene-encased NiO_x during the postmetallization annealing. The observed low light output is therefore correlated to the phase change induced transmittance loss in the NiO_x/graphene electrode. These findings provide new insights into the behavior of different interlayers under processing conditions that will be useful for the future development of opto-electronic devices with graphene-based electrodes.

KEYWORDS: *graphene, ohmic contact, interlayer, annealing, NiO_x/graphene, light-emitting diode*

1. INTRODUCTION

Recently, graphene has drawn a widespread research interest due to its fascinating properties such as high optical transparency, superior electrical and thermal conductivities, mechanical flexibility, and giant intrinsic carrier mobility. Accordingly, two-dimensional graphene sheet is considered as a next-generation transparent conductive electrode in lieu of conventional indium tin oxide (ITO) for applications in optoelectronic devices such as solar cells and light-emitting diodes (LEDs).[1−3] It has been demonstrated that graphene can be applied to p-GaN layer in InGaN/GaN LEDs as a transparent current spreading electrode, in spite of difficulties in accomplishing favorable interfacial properties at the graphene/p-GaN contact.[4−7] The focal concerns associated with the integration of pristine graphene directly with p-GaN are the formation of Schottky barrier height ($q\varphi_B$) at the interface between the two as a result of large difference in work function (Φ) and graphene's high sheet resistance (R_{sh}). In principle, the $q\varphi_B$ of the graphene contact to the p-GaN is estimated to be ~3 eV, based on the difference between the theoretical Φ of graphene (Φ_{GR}~4.5 eV) and p-GaN (Φ_{GaN} ~7.5 eV). Thus, for the development of reliable devices it is indispensable that the graphene-GaN contact ought to have low specific contact resistance (ρ_c) and lowest possible barrier. Furthermore, interface engineering is becoming a vital part of device fabrication in order to further advance graphene's application in optoelectronic devices.

Our recent study has demonstrated that the tuning of graphene Φ and use of ultrathin Au interlayer improves the interfacial contact properties between the graphene and p-GaN by lowering the $q\varphi_B$ and ρ_c.[5] However, the $AuCl_3$ treatment used to tailor-make the graphene to yield low R_{sh} and high Φ reduces the transparency of the graphene to some extent because of light scattering by the incorporation of unintentional

Received: November 7, 2012
Accepted: January 10, 2013
Published: January 10, 2013

© 2013 American Chemical Society

Au nanoparticles during the charge transfer doping process.[5,8] Lee et al.[4,9] emphasized that the insertion of thin metal interlayer (viz. Ni or Ni/Au) at the graphene−GaN interface is vital for improving the device performance despite a 10−20% loss in transmittance. A recent study that suggests the use of Ag nanoparticles on graphene to enhance the reliability of graphene electrode in GaN LED made evident that this approach would also lead to loss in optical transmittance.[6] Although the implementation of GaN-based LEDs with graphene anode is realized through these methods, there is still very little known about the interface physics at the graphene/GaN junction. Therefore, it is imperative and timely to explore the carrier transport across the graphene/p-GaN interface and its modification in the event of interface engineering. In addition, more attention needs to be given in exploring yet another promising interlayer for a reliable device structure.

Herein, first the effects of various ultrathin interlayers (Au, Ni, and NiO_x) and high-temperature postmetallization anneal on the ρ_c of graphene/p-GaN interface are evaluated using circular transmission line model (CTLM). The idea of using such interlayers having an intermediate work function ($\Phi_{GR} < \Phi_{metal} < \Phi_{GaN}$) is to reduce the barrier height and/or barrier width at the graphene/p-GaN interface, allowing for the formation of low resistance ohmic contacts. Indeed, this tactic is found practical from the analyses of the $I-V$ curves. The ρ_c of graphene/p-GaN contact at 300 K is reduced down to ~2×10^{-1} from 8.8×10^{-1} Ω cm^2 when such interlayers are used. In addition, the temperature dependent current−voltage ($I-V-T$) measurements revealed that the prevailing carrier transport mechanism across the junction is modified from thermionic field emission (TFE) to tunneling by the introduction of interlayers. InGaN/GaN LEDs with graphene and NiO_x/graphene (here after it will be referred to be NiO_x/GR) electrodes are fabricated to substantiate the above result.

2. EXPERIMENTAL SECTION

2.1. Formation of Graphene/p-GaN Circular Contact Structures. A 1.2 μm thick p-GaN was intentionally grown on a *c*-plane sapphire substrate by metalorganic chemical vapor deposition. The free hole concentration (p) and the Hall mobility (μ) of the p-GaN layer were determined to be 6.9×10^{17} cm^{-3} and 5.7 cm^2 v^{-1} s^{-1}, respectively, from the Hall measurements conducted at room temperature. Secondary ion mass spectroscopy (SIMS) depth profiling analysis showed a homogeneous distribution of Mg acceptors with concentrations as high as 8.5×10^{19} atoms/cc (not shown here). The 2 in. epilayer wafer was diced into pieces of 10 × 10 mm, and three of them were coated with a 2 nm Au, Ni, and NiO_x (which was obtained via rapid thermal annealing (RTA) of Ni film in oxygen ambient at 500 °C for 60 s) by electron beam evaporation. Graphene grown by chemical vapor deposition on Ni or Cu was then transferred onto each substrate via a wet-etch process as described in our earlier work.[5] The CTLM test patterns were formed using photolithography and inductively coupled plasma reactive ion etching (ICP/RIE). In this process, the graphene and underlying metal were etched out successively with O_2 and CF_4:Ar:O_2 plasma, respectively. Briefly, the contact pattern employed for this study comprised of six rings of varying inner radii (5, 10, 15, 20, 35, and 45 μm), while maintaining a constant outer radius of 200 μm. The postmetallization annealing of the contacts was conducted in an RTA system at 450 or 550 °C for an extended period of 5−10 min (which is reported to be the optimal conditions) under N_2 or Ar ambient.

2.2. Device Fabrication. InGaN/GaN LEDs with Ni/Au, GR, and NiO_x/GR electrodes were fabricated by a similar procedure described in reference 10. However, a modified graphene-transfer process that gives uniform coverage with less number of damages has been adopted in the present study. Briefly, the graphene was coated with a polymethylmethacrylate (PMMA) (4% in toluene), which was allowed to dry naturally overnight instead of immediate baking on a hot plate. The PMMA-covered graphene was then released from its native substrate through etching of metal catalyst in a $FeCl_3$ solution. The PMMA/graphene stack was then transferred successively to three to four deionized water baths in 10 min durations to ensure the elimination of chemical residues result from the etching process. The PMMA-supported graphene was then transferred to the prepatterned LED substrates, allowed to dry overnight naturally, and annealed at 180 °C for 30 min in a forced convection oven. Finally, the PMMA was removed from the graphene in a warm acetone for several hours. This modified procedure gives comparatively better transfer yield in view of transferred graphene's geometry and evenness, although the PMMA removal process introduces occasional damages to graphene, creating cracks or holes (see Figure S1 in the Supporting Information). Furthermore, it is worth to mention that our implemented idea of using prepatterned substrates (performing mesa etching prior to graphene transfer) in the fabrication of LEDs with graphene electrode has been shown to be effective to limit the process-induced damages to the graphene and accomplish reliable device performances.[11]

2.3. Characterization. The surface topography of graphene films was probed by atomic force microscopy (AFM, Digital Instruments, Nanoscope IV A) in tapping mode. Raman spectroscopy (Renishaw) was used to characterize the structural quality of the graphene before and after transfer. A He−Ne laser with a wavelength of 632.8 nm was used for excitation and the beam was focused through a 100x magnifying objective of the Leica microscope. Field emission scanning electron microscopy (FESEM, Hitachi S-4800) was used to probe the interface microstructure of the graphene/metal/p-GaN contacts. Room-temperature $I-V$ measurements were carried out before and after postmetallization annealing and the $I-V-T$ measurements were carried out on annealed contacts using a precision semiconductor parameter analyzer for different temperatures in the range between 200 and 500 K. Combined X-ray and ultraviolet photoelectron spectroscopy (XPS/UPS) measurements were performed on an AXIS-NOVA, Kratos spectrometer with a monochromized Al Kα X-ray source (1486.6 eV). He I discharge lamp (hυ = 21.22 eV) was used as an excitation source for UPS measurements and the value of Φ was measured from the secondary-electron cutoff using Au metal as a reference. The Fermi level was determined from the Fermi edge of the Au metal. The optical transmittance measurements were carried out by using a JASCO V-570 ultraviolet−visible−near-infrared (UV−visible−NIR) spectrophotometer. Current−voltage ($I-V$) and light output-current ($L-I$) measurements on the LED chips were carried out using a probe station system.

3. RESULTS AND DISCUSSION

Figure 1 shows the $I-V$ curves obtained on graphene/p-GaN contacts before and after RTA process. It can be noticed that the $I-V$ curve of the contact before RTA is nonlinear, suggesting strong rectification at the interface, a typical propensity revealed for most semiconductor−graphene interfaces because of a charge-transfer-favored shift in graphene's Fermi level (E_F).[12] A recent theoretical investigation on graphene-GaN contacts elucidated that the charge transfer leads to a self-adaptive shift of the E_F and consequently lowers the barrier height for graphene contact on both n- and p-type GaN.[13] However, in practice, many factors could contribute to the observed nonlinear $I-V$ behavior such as the adhesion between the two layers, R_s of the graphene, and evenness and limpidness of graphene's surface in contact with the GaN. Unlike evaporated metal contacts to semiconductors where the interface is largely characterized by chemisorption, the wet transfer route commonly employed to date for the integration of graphene with foreign substrate surfaces limits the adhesion to be comparatively weak on account of van der Walls

dx.doi.org/10.1021/am3026079 | ACS Appl. Mater. Interfaces 2013, 5, 958−964

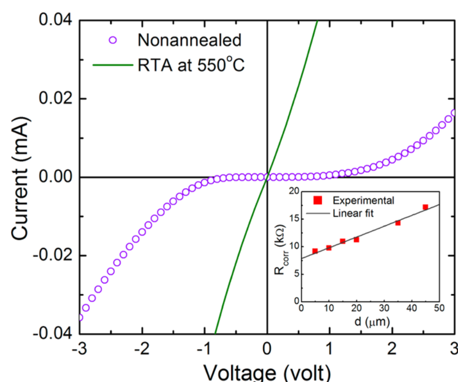

Figure 1. $I-V$ characteristics of typical graphene/p-GaN contacts before and after RTA. The inset shows the corrected total resistance verses gap spacing (d) calculated from the $I-V$ curves measured for the same set of contacts.

physisorption. In most cases, this gives rise to a dead space between the graphene and the substrate.[14] However, the adhesion can be reinforced by thermal annealing, which is also known to eradicate the defects in graphene and residual PMMA contaminants.[7,14−16] The analysis of C 1s core level spectra of graphene before and after RTA showed that annealing even for a short period of 5−10 min at 450 °C considerably removes the PMMA contaminants from the surface of the graphene (see Figure S2 in the Supporting Information). Referring to recent studies,[7,14] it is worth taking into consideration that annealing of graphene on GaN and/or SiO_2 at elevated temperatures does not cause any unfavorable structural modifications in the graphene. Furthermore, because the annealing conditions used in our experiments are reminiscent of the conditions used by Zhang et al.[7] for the graphene on GaN, any interfacial reactions between the graphene and GaN can be ruled out and graphene is expected to retain its structural quality.

A comparison of the $I-V$ curves before and after RTA clearly indicates that the contact after annealing is significantly less rectifying with higher current at any fixed voltage. The observed improvements in the contact characteristics can be ascribed to the enhanced adhesion between the two layers. For these contacts, a ρ_c of 8.8×10^{-1} Ω cm^2 is estimated from the gap spacing dependence of resistance (inset of Figure 1). The calculated ρ_c is on the first sight two or three orders higher than for the commonly used electrode materials ITO and Ni/Au. However, with the use of additional highly Mg-doped p-GaN (commonly referred to as p^{++}-GaN) or tunneling layers the ρ_c can be further improved. In addition, a highly reliable graphene transfer process has to be adopted in order to produce contacts of utmost quality.

The effect of introducing ultrathin metal interlayer between the graphene and p-GaN on the contact characteristics is systematically studied by employing high Φ metals Au (Φ = 5.1 eV) and Ni (Φ = 5.15 eV), and a transparent conductive metal-oxide NiO_x as they are routinely used for ohmic contact formation in GaN-based devices.[17] With thin metal film at the interface, the following behaviors are anticipated; rectification behavior of the contact can be eliminated by reducing the barrier width and an effective work function in the order of metal work function can be achieved because of charge transfer that could occur exclusively at the metal/graphene interface.[18] Figure 2a compares the experimental $I-V$ curves of the contacts with different interlayers studied. It should be noted that the contacts exhibit perfectly ohmic behavior even at low voltage ranges irrespective to the type of interlayer. Moreover, the graphene/Au/p-GaN configuration exhibited a lowest ρ_c of 1.96×10^{-1} Ω cm^2, whereas other two contacts had comparable values well within the experimental error. The obtained ρ_c value is very comparable to the value of 6×10^{-1} Ω cm^2 reported for a graphene/p-GaN contact tailored with thin Ni(1 nm)/Au(1 nm) interlayer wherein the graphene used was a monolayer boasting a R_{sh} of 100−200 ohm/square.[4]

The similarity of the curves with no significant variations in the current levels among the three different contact configurations studied imply that the work function difference ($\Phi_{GR} - \Phi_{metal}$) is not the only factor determining the ohmic behavior with low ρ_c. If this was the reason then the contacts made with either Ni or NiO_x interlayer should outperformed the one made with Au interlayer, because Au has been shown to be poor in altering the graphene's Φ compared with Ni.[18] Moreover, the Φ of the NiO_x/GR stack is estimated to be 5.53 eV using the ultraviolet photoemission spectroscopy (see Figure S3 in the Supporting Information). This anomaly can be explained in the light of physiochemical processes that occur at the metal/p-GaN interface during high-temperature annealing. It has been consistently revealed that metal/p-GaN interface tend to undergo substantial modifications under postmetalliza-

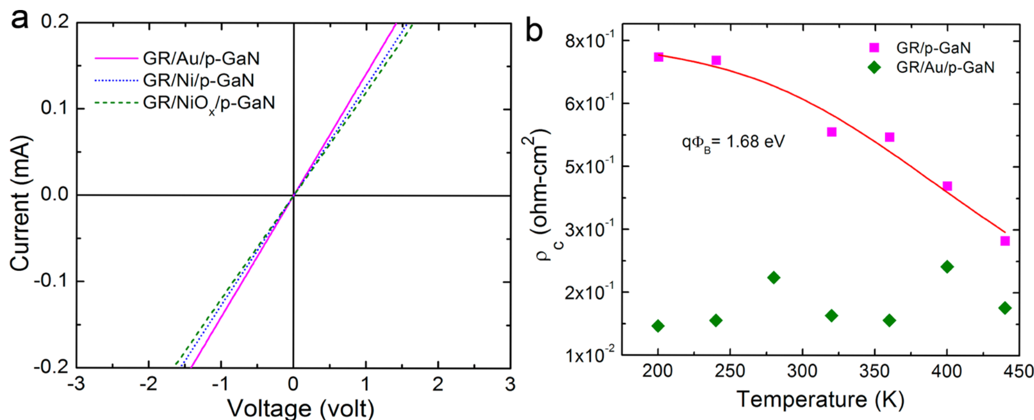

Figure 2. (a) $I-V$ characteristics of the graphene/p-GaN contacts modified with different interlayers. (b) Temperature dependence of specific contact resistance for typical graphene/p-GaN and graphene/metal/p-GaN contact configurations. The solid red line indicates the theoretical fit to experimental data based on TFE model.

tion annealing.[17,19−22] For instance, Ga out-diffusion induced local increase in the carrier concentration and changes in the microstructure due to interfacial reactions that occur during annealing between metal and p-GaN are shown to be liable for enhanced ohmic characteristics. According to Schottky theory, while the barrier height relies on the work function the barrier width hinges on the free carrier concentration. A high free carrier concentration is known to offer narrow space-charge region width which could favor carrier tunneling across the interface.[23]

To understand the real mechanism at play, the temperature dependent *I*−*V* characteristics of the contacts are studied. Band conduction is considered as a dominant mechanism of carrier transport in graphene/GaN contacts, because a semilogarithemic plot of electrical resistivity of p-GaN as a function of inverse of temperature followed the Arrhenius relation (see Figure S4 in the Supporting Information). Figure 2b shows the temperature dependence of ρ_c for typical graphene/p-GaN and graphene/metal/p-GaN contacts. A comparison of the two plots indicates that the variation in ρ_c with temperature is modified by the presence of interlayer. In the case of graphene/p-GaN direct contact, the ρ_c decreases with increasing measurement temperature, a typical behavior of the contacts characterized by thermionic emission or TFE theory.[19,24] By fitting the experimental data to the above models, the $q\varphi_B$ is estimated to be 1.68 eV, which is less than the value predicted from traditional Schottky-Mott theory. This difference stems from the fact that the E_F of graphene is highly susceptible to change when it makes a direct contact with semiconductors because of charge transfer across the interface, which is quite different from that of conventional metal/semiconductor contacts where the E_F of the metal stays constant due to a high density of states at the E_F.[12,13] On the other hand, the ρ_c is found to be virtually insensitive to the temperature for graphene/metal/p-GaN contacts. This behavior is characterized by the field-emission (tunneling) theory as $\rho_c \alpha \exp^{\Phi_B/E_{oo}}$. On the basis of these results, it is reasonable to state that the ohmic nature of the graphene/metal/p-GaN contacts and associated low ρ_c could be ascribed to the enhanced carrier tunneling due to reduced barrier width. Moreover, at the graphene/p-GaN interface, the metal interlayers upon annealing tend to form nanodots as shown in Figure 3. It should be noted that such a discontinuous metal film could result a strong enhancement in the electric field at the metal/semiconductor interface and consequently lower the $q\varphi_B$.[17] Therefore, the improvements in the contact characteristics could also be ascribed to the formation of inhomogeneous $q\varphi_B$ at the metal/p-GaN interface.[10,17] In addition, the high solubility tendency of Ga in Au could be the probable reason for the comparatively better ohmic characteristics obtained with Au interlayer.[22,25]

An interesting finding from the present investigation is the realization of ohmic contacts with NiO_x interlayer. Formation of p-type NiO_x interfacial layer during annealing of Ni/Au and Ni/ITO or Ni/ZnO in oxygen atmosphere is a well-known cause in the realization of low resistance ohmic contacts to p-GaN.[17,26−28] In these contacts, the NiO_x formed via postoxidation annealing is characterized by Ni vacancies and/or oxygen interstitials with high carrier concentration. Consequently, this interfacial layer is believed to offer low barrier for charge carrier injection and therefore held responsible for the ohmic contact formation, although a number of added feasible mechanisms are accentuated in the literature.[17,21,22] In addition, being a transparent conductive

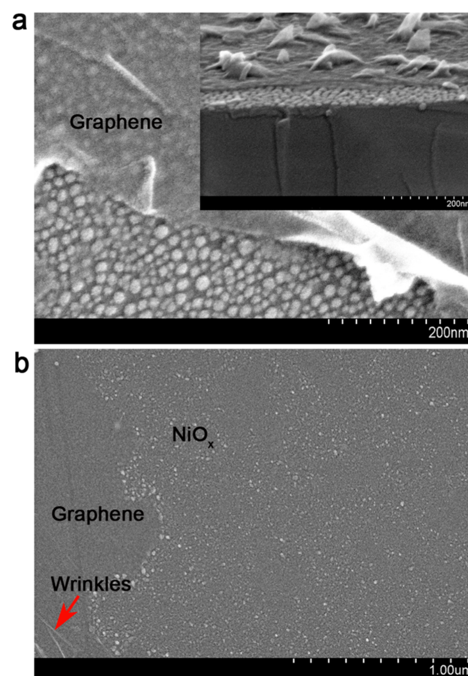

Figure 3. (a) FESEM images of a graphene-covered 2 nm Au film revealing the formation of nanodots after being annealed at 550 °C. The inset is the cross-section view of a typical graphene/Au/p-GaN interface subjected to RTA. (b) Surface morphology of a 2 nm NiO_x film indicating the granular microstructure of the film. The image is obtained at the graphene−film boundary at random sites.

oxide, the transparency of even 10 nm NiO_x film is much higher than for a 2 nm Au and Ni films (see Figure S5 in the Supporting Information). It is also found that the NiO_x(2 nm)/GR stack (consisting of monolayer graphene) offers transmittance as high as 95%. These facts together with the observed ohmic contact formation imply that the NiO_x/GR would be an ideal choice of electrode, which may result in devices of reasonable electrical and optical performances. Since the device with Au interlayer has already been dealt in our earlier study only the NiO_x case is considered for the present investigation.

From this point of view, a systematic study has been made wherein the electrical and optical characteristics of InGaN/GaN blue LEDs with translucent Ni/Au, graphene, and NiO_x/GR electrodes were compared. From the *I*−*V* characteristics of the devices shown in Figure 4a, it is evident that the forward voltage of the device made with pristine graphene is comparatively high (4.5 V at 20 mA) due to high $q\varphi_B$ of graphene/p-GaN contact as discussed earlier. The forward voltage obtained in this study is analogous to the values reported in the literature.[6] Interestingly the device with NiO_x/GR electrode offered a forward voltage of 3.16 V, which is very close to the value of 3.04 V obtained for a reference device with Ni/Au electrode. It should be noted that the forward voltage (3.16 V) attained in this study is the lowest value ever reported for a GaN LED with graphene electrode. Moreover, the *I*−*V* curve measured on a device with only NiO_x made obvious that the observed low forward voltage is a direct consequence of the NiO_x interlayer. However, only NiO_x cannot act as a current spreading electrode as evidenced from the optical image (see inset of Figure 4a) of a corresponding device.

The light output powers from the respective LEDs are compared in Figure 4b. The results provided here is the average data of more than ten measurements made on each sample. It is

dx.doi.org/10.1021/am3026079 | ACS Appl. Mater. Interfaces 2013, 5, 958−964

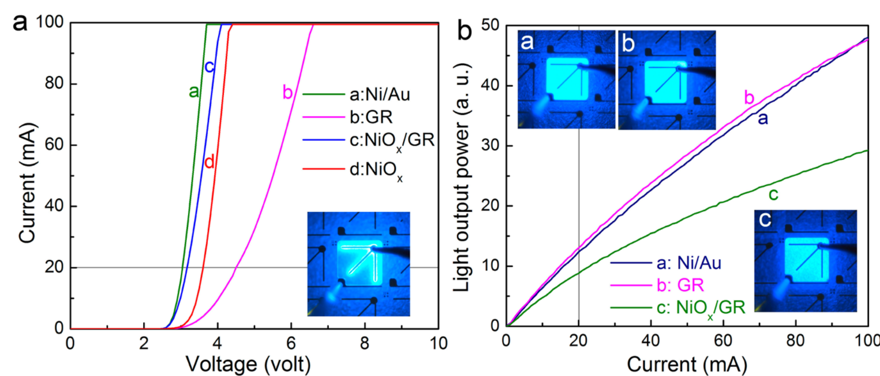

Figure 4. (a) Current−voltage characteristics of GaN LEDs studied with different electrodes. The inset is the optical image captured during the light emission from a device with only NiO_x. (b) Average light output power as a function of injection current measured on unpackaged LED chips of different electrodes. The current spreading ability of graphene can be directly evidenced by comparing the optical images (captured at an injection current of 200 μA) given in a and b.

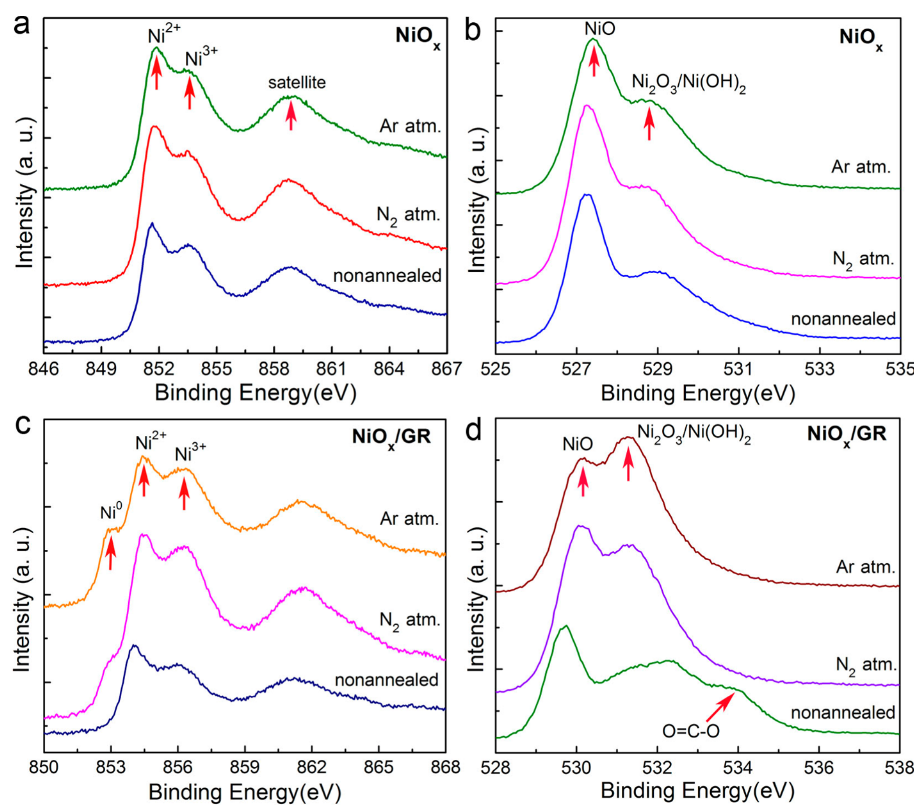

Figure 5. (a, c) XPS Ni $2p_{3/2}$ and (b, d) O1s core-level spectra of NiO_x and NiO_x/GR before and after thermal annealing at 450 °C under two different ambient. The peak at 534 eV designated to O−C═O in d originates from the PMMA residue.

observed that in spite of large contact resistance, the LED with graphene electrode offered light output power comparable to that of the reference LED. However, the large difference in power consumption ($P = VI$ = 61 and 90 mW, respectively, for the devices with Ni/Au and graphene electrodes) signifies that the power efficiency[29] ($\eta = P/VI$, where P is the optical output power) of the former is yet lower (approximately 30% at an injection current of 20 mA) than the reference LED. This is indeed further evidenced from the comparable transmittance of the Ni/Au and graphene employed in this study (see Figure S5 in the Supporting Information). By revisiting Figure 4b one can notice that contrary to expectations the device with NiO_x/GR electrode offered a low light output. This abnormality is caused because of the post-annealing induced structural modifications and associated transmittance degradation in the NiO_x/GR stack as described below.

The device with NiO_x/graphene turned out to be relatively opaque after post annealing process, providing the first indication that the poor light output is likely a result of anneal-induced degradation in the optical transparency of NiO_x/GR stack. To further elucidate this observation, we recorded transmittance spectra on the NiO_x and NiO_x/GR films before and after annealing (see Figure S5 in the Supporting Information). It is observed that the transmittance of the NiO_x/GR stack is critically reduced upon post annealing, while the NiO_x film has preserved its high transparency. In an attempt to understand the mechanism leading to such disparate behavior, we performed XPS studies on each sample. Figure 5

shows the Ni 2p and O 1s core-level spectra of the NiO_x and NiO_x/GR samples. The Ni $2p_{3/2}$ spectrum of NiO_x film (Figure 5a) exhibits three characteristic peaks relative to the Ni^{2+} and Ni^{3+} electronic states and their satellite in the NiO_x system. The coexistence of the two bonding states is typical for the NiO_x films prepared by any method and exposed to ambient conditions.[30−33] The corresponding O1s spectrum further confirms the existence of two different phases. However, there are large uncertainties in elucidating whether the Ni^{3+} state is a consequence of the existence of Ni_2O_3 phase or the surface Ni hydroxide ($Ni(OH)_2$).[31] The absence of Ni^0 (metallic Ni) peak signifies that the entire Ni film is converted into NiO_x during the oxidation process. The Ni $2p_{3/2}$ and O1s spectra of the annealed NiO_x films resemble to that of the nonannealed one except a slight shift in the peak positions toward the higher binding energy and variations in the peak area for the two components. Suffice here to conclude from the above results that no phase transformation occurs in the NiO_x film during the post annealing.

The NiO_x/GR stack, on the other hand, showed a clear disparity in its chemical environment upon post annealing compared to the nonannealed film. For the annealed sample, a new peak at 852.9 eV emerged in the Ni $2p_{3/2}$ spectrum, whereas the relative intensity of the Ni^{3+} peak increased in the O 1s spectrum. The binding energy of 852.9 eV agrees well with that of metallic Ni and Ni_3C.[31,34] However, the formation of carbide phase is excluded due to the following reasons; (i) the adventitious C−Ni peak is absent at 283.5 eV in the C1s spectra of the NiO_x/GR stacks (see Figure S2 in the Supporting Information) before and after annealing and (ii) it is demonstrated that the graphene is stable up to 650 °C on a catalytic Ni surface and never converts into a carbide below this temperature.[35] Considering the above facts, the peak at 852.9 eV is certainly attributed to metallic Ni. The formation of metallic Ni along with the changes in the relative intensity ratio of Ni^{3+} to Ni^{2+} could be likely due to the oxide reduction upon annealing through the forward disproportionation reaction as put forward by Chien et al.[36] Considering the fact that the catalytic NiO_x has a greater propensity to form surface hydroxide in atmospheric conditions,[31,37] the intensity variations observed for the Ni^{3+} component can also be correlated to the formation of $Ni(OH)_2$ during the graphene transfer process which involved exposure of NiO_x to water and humid ambience. Regardless of the nature of the mechanism involved, both the formation of metallic Ni and the increase of Ni^{3+} could diminish the optical transparency of the NiO_x/GR stack. If this is the case, why does phase change takes place only in passivated NiO_x (assuming the graphene a protective layer as delineated in ref 38), whereas the exposed NiO_x surface is stable upon annealing? A recent study on NiO-graphene composite has revealed the formation of oxygen bridges between NiO and graphene by a pinning effect of hydroxyl groups on the Ni atoms of NiO.[39] Is such a bonding feasible at the graphene/NiO_x interface on rapid thermal annealing? Further thermal and interface studies are needed to address these issues, understand the nature of the interaction between the NiO_x and graphene, and discriminate the behavior of NiO_x/GR as a function of post oxidation and annealing conditions. It is also evident from Figure 5 that the annealing in N_2 and Ar ambient results similar behavior with the consequences being greater for the latter.

4. CONCLUSIONS

To summarize, we evaluated the current transport across the graphene/p-GaN contact and its modification with respect to Au, Ni, and NiO_x interlayers and carried out a case study addressing the feasibility of using NiO_x/graphene electrode to InGaN/GaN LED. The results signify that the use of interlayer and postmetallization annealing leads to the formation of ohmic contact with improved contact resistance. The temperature dependence of the specific contact resistance revealed that the carrier transport in graphene/metal/p-GaN contacts is governed by tunneling. The contacts with any of the interlayer presented comparable characteristics superior to that of direct graphene/p-GaN contact owing to anneal induced interfacial reactions between the metal and GaN. This indicates that the change in work function theoretically predicted for the graphene on metals is not the only factor determining the contact characteristics when the contact is subjected to postmetallization annealing. InGaN/GaN LED with NiO_x/graphene as a current spreading electrode offered a low forward voltage of 3.16 V, which is close to that of 3.04 V obtained for a device with translucent Ni/Au. On the other hand, post annealing led to unfavorable phase changes in the NiO_x/GR stack and consequently hampered the light output from the respective device. Even so, the low forward voltage achieved with the NiO_x interlayer and high transparency of the NiO_x/GR stack suggests that there is still room for the overall device efficiency enhancement by further optimization of the processing conditions. Besides its interest for GaN LEDs, NiO_x is established to have great application potential in many devices such as organic LEDs and polymer photovoltaics wherein it performs as a buffer layer between the anode and hole transport layer. Because graphene is already being used as an anode in these devices, the phase transformation revealed for graphene-encased NiO_x in this study is a pivotal finding and would instigate further research in this field.

■ ASSOCIATED CONTENT

Supporting Information

Surface morphology and Raman spectra of transferred graphene (Figure S1), XPS C1s spectra of NiO_x/graphene (Figure S2), UPS spectra of the NiO_x/GR stack (Figure S3), inverse temperature dependence of the electrical resistivity of the p-GaN (Figure S4), and optical transmittance spectra of different metal interlayers, graphene, NiO_x/graphene stacks (Figure S5). This material is available free of charge via the Internet at http://pubs.acs.org/.

■ AUTHOR INFORMATION

Corresponding Author

*E-mail: chhong@jbnu.ac.kr.

Author Contributions

The manuscript was written through contributions of all authors. All authors have given approval to the final version of the manuscript

Notes

The authors declare no competing financial interest.

■ ACKNOWLEDGMENTS

This work was financially supported by Ministry of Knowledge Economy (MKE) and Korea Institute for Advancement of Technology (KIAT) through the Workforce Development Program in Strategic Technology and by Priority Research

Center Program through the National Research Foundation of Korea (NRF) funded by the Ministry of Education, Science, and Technology (2011-0027956).

■ REFERENCES

(1) Jo, G.; Choe, M.; Cho, C. Y.; Kim, J. H.; Park, W.; Lee, S.; Hong, W. K.; Kim, T. W.; Park, S. J.; Hong, B. H.; Kahng, Y. H.; Lee, T. *Nanotechnology* **2010**, *21*, 175201.
(2) Huang, X.; Zeng, Z.; Fan, Z.; Liu, J.; Zhang, H. *Adv. Mater.* **2012**, *24*, 5979−6004.
(3) Han, T. H.; Lee, Y.; Choi, M. R.; Woo, S. H.; Bae, S. H.; Hong, B. H.; Ahn, J. H.; Lee, T. W. *Nat. Photon.* **2012**, *6*, 105−110.
(4) Lee, J. M.; Jeong, H. Y.; Choi, K. J.; Park, W. I. *Appl. Phys. Lett.* **2011**, *99*, 041115.
(5) Chandramohan, S.; Kang, J. H.; Katharria, Y. S.; Han, N.; Beak, Y. S.; Ko, K. B.; Park, J. B.; Kim, H. K.; Suh, E. K.; Hong, C. H. *Appl. Phys. Lett.* **2012**, *100*, 023502.
(6) Shim, J. P; Kim, D. H.; Choe, M.; Lee, T.; Park, S. J.; Lee, D. S. *Nanotechnology* **2012**, *23*, 255201.
(7) Zhang, Y.; Wang, L.; Li, X.; Yi, X.; Zhang, N.; Li, J.; Zhu, H.; Wang, G. *J. Appl. Phys.* **2012**, *111*, 114501.
(8) Choe, M.; Cho, C. Y.; Shim, J. P.; Park, W.; Lim, S. K.; Hong, W. K.; Lee, B. H.; Lee, D. S.; Park, S. J.; Lee, T. *Appl. Phys. Lett.* **2012**, *101*, 031115.
(9) Lee, J. M.; Yi, J.; Lee, W. W.; Jeong, H. Y.; Jung, T.; Kim, Y.; Park, W. I. *Appl. Phys. Lett.* **2012**, *100*, 061107.
(10) Chandramohan, S.; Kang, J. H.; Katharria, Y. S.; Han, N.; Beak, Y. S.; Ko, K. B.; Park, J. B.; Ryu, B. D.; Kim, H. K.; Suh, E. K.; Hong, C. H. *J. Phys. D: Appl. Phys.* **2012**, *45*, 145101.
(11) Joo, K.; Jerng, S. K.; Kim, Y. S.; Kim, B.; Moon, S.; Moon, D.; Lee, G. D.; Song, Y. K.; Chun, S. H.; Yoon, E. *Nanotechnology* **2012**, *23*, 425302.
(12) Tongay, S.; Lemaitre, M.; Miao, X.; Gila, B.; Appleton, B. R.; Hebard, A. F. *Phys. Rev. X* **2012**, *2*, 011002.
(13) Zhong, H.; Liu, Z.; Xu, G.; Fan, Y.; Wang, J.; Zhang, X.; Liu, L.; Xu, K.; Yang, H. *Appl. Phys. Lett.* **2012**, *100*, 122108.
(14) Cheng, Z.; Zhou, Q.; Wang, C.; Li, Q.; Wang, C.; Fang, Y. *Nano Lett.* **2011**, *11*, 767−771.
(15) Pirkle, A.; Chan, J.; Venugopal, A.; Hinojos, D.; Magnuson, C. W.; McDonnell, S.; Colombo, L.; Vogel, E. M.; Ruoff, R. S.; Wallace, R. M. *Appl. Phys. Lett.* **2011**, *99*, 122108.
(16) Ni, Z. H.; Wang, H. M.; Ma, Y.; Kasim, J.; Wu, Y. H.; Shen, Z. X. *ACS Nano* **2008**, *2*, 1033−1039.
(17) Song, J. O.; Ha, J. S.; Seong, T. Y. *IEEE Trans. Elect. Devices* **2010**, *57*, 42−59.
(18) Song, S. M.; Park, J. K.; Sul, O. J.; Cho, B. J. *Nano Lett.* **2012**, *12*, 3887−3892.
(19) Iucolano, F.; Roccaforte, F.; Alberti, A.; Bongiorno, C.; Franco, S. D.; Raineri, V. *J. Appl. Phys.* **2006**, *100*, 123706.
(20) Ruterana, P.; Albrecht, M.; Neugebauer, J. *Nitride Semiconductors: Handbook on Materials and Devices*; Wiley-VCH Verlag GmbH & Co.: Weinheim, Germany, 2001; p 495.
(21) Greco, G.; Prystawko, P.; Leszczynski, M.; Nigro, R. L.; Raineri, V.; Roccaforte, F. *J. Appl. Phys.* **2011**, *110*, 123703.
(22) Koziorowska, J. S.; Grzanka, S.; Staszewska, E. L.; Piotrzkowski, R.; Nowak, G.; Leszczynski, M.; Perlin, P.; Talik, E.; Kozubowski, J.; Krukowski, S. *Solid-State Electron.* **2010**, *54*, 701−709.
(23) Schroder, D. K. *Semiconductor Material and Device Characterization*; John Wiley & Sons: New York, 2006; p 129.
(24) Blank, T. V.; Gol'dberg, Y. A.; Konstantinov, O. V.; Nikitin, V. G.; Posse, E. A. *Semiconductors* **2006**, *40*, 1173−1177.
(25) Liu, Y. J.; Huang, C. C.; Chen, T. Y.; Hsu, C. S.; Liou, J. K.; Tsai, T. Y.; Liu, W. C. *Opt. Express* **2011**, *19*, 14662.
(26) Ho, J. K.; Jong, C. S.; Chiu, C. C.; Huang, C. N.; Chen, C. Y.; Shih, K. K. *Appl. Phys. Lett.* **1999**, *74*, 1275.
(27) Horng, R. H.; Wuu, D. S.; Lien, Y. C.; Lan, W. H. *Appl. Phys. Lett.* **2001**, *79*, 2925−2927.
(28) Song, J. O.; Kim, K. K.; Park, S. J.; Seong, T. Y. *Appl. Phys. Lett.* **2003**, *83*, 479−481.
(29) Schubert, E. F. *Light-Emitting Diodes*; Cambridge University Press: Cambridge, U.K., 2006; p 87.
(30) Awais, M.; Rahman, M.; MacElroy, J. M. D.; Coburn, N.; Dini, D.; Vos, J. G.; Dowling, D. P. *Surf. Coat. Technol.* **2010**, *204*, 2729−2736.
(31) Greiner, M. T.; Helander, M. G.; Wang, Z. B.; Tang, W. M.; Lu, Z. H. *J. Phys. Chem. C* **2010**, *114*, 19777.
(32) Yun, D. J.; Rhee, S. W. *J. Vac. Sci. Technol. B* **2008**, *26*, 1787−1793.
(33) Gupta, P.; Dutta, T.; Mal, S.; Narayan, J. *J. Appl. Phys.* **2012**, *111*, 013706.
(34) Chu, J. H.; Kwak, J.; Kwon, T. Y.; Park, S. D.; Go, H.; Kim, S. Y.; Park, K.; Kang, S.; Kwon, S. Y. *ACS Appl. Mater. Interfaces* **2012**, *4*, 1777−1782.
(35) Lahiri, J.; Miller, T. S.; Ross, A. J.; Adamska, L.; Oleynik, I. I.; Batzill, M. *New J. Phys.* **2011**, *13*, 025001.
(36) Chien, F. S. S.; Wu, Y. T.; Lai, G. L.; Lai, Y. H. *Appl. Phys. Lett.* **2011**, *98*, 153513.
(37) Korošec, R. C.; Bukovec, P. *Acta Chim. Slov.* **2006**, *53*, 136−147.
(38) Nayak, P. K.; Hsu, C. J.; Wang, S. C.; Sung, J. C.; Huang, J. L. *Thin Solid Films* **2012**, http://dx.doi.org/10.1016/j.tsf.2012.03.067.
(39) Zhou, G.; Wang, D. W.; Yin, L. C.; Li, N.; Li, F.; Cheng, H. M. *ACS Nano* **2012**, *6*, 3214−3223.